Universität Münster

Statistical model fits of hadron ratios in nucleus-nucleus collisions

A Bachelor's thesis

by

Thilo Grüntges

Student number: 526398

Course of Study: Dual-subject Bachelor mathematics and physics

First assessor: Prof. Dr. Anton Andronic

Second assessor: Apl. Prof. Dr. Christian Klein-Bösing

Münster, 4th May 2025

Contents

1 Introduction

Particle physics is the study of the fundamental particles and forces that constitute matter. The primary experimental way in which these have been discovered and their properties measured are the controlled environments of high-energy particle colliders. Inside them particles are accelerated to velocities close to the speed of light and then collided, which leads to the creation of new particles from the energy of the collision. All outgoing particles are then measured by surrounding particle detectors. Inside this data physicists search for signs of new particles and processes that might occur under the extreme conditions present in the collisions.
Although the detector only measures the outcome of the collision and not the occurring processes themselves. Models of the occurring processes can be tested through simulating them, for example through Monte-Carlo event generators, and comparing the results of the simulations to the data collected in accelerator experiments.
In the last decades thermal (statistical) models have shown remarkable success in describing the ratios of hadron yields in high energy nucleus-nucleus collisions. The thermal model describes the yields of produced particles based only on a few thermal parameters present at the chemical freeze-out of the collision. In this thesis, results of a thermal model are compared with the measured particle ratios of a wide range of energies. With this data one of these thermal parameters, the temperature, is determined.
First the general theory of particle collisions is described in section 2. Then the experimental approach for the collection of the experimental data is laid out in section 3. Section 4 presents the thermal model used to calculate the theoretical data and section 5 elaborates on how the thermal parameter is determined through fitting of the data. Afterwards section 6 gives the mathematical background of the fitting procedure and section 7 a description of the program used for all the calculations. This program is written in python and can be received upon requested from A. Andronic. The results of the fits are analysed and discussed in section 8. Finally, concluding thoughts will be presented in section 9.

2 Theoretical Background

This chapter explores the fundamental theory behind high-energy particle collisions, which is based on the Standard Model of particle physics. The Standard Model provides our current understanding of the elementary building blocks of matter and three of the four fundamental forces of nature: the electromagnetic, weak, and strong interactions. Gravity, while a fundamental force, is not included in the Standard Model. However, at (sub)atomic scales, its effects are negligible.
Section 2.1 describes the constituents of the standard model and the following subsections explore the fundamental theories used in the description of Relativistic nucleus-nucleus Collisions.

2.1 The Standard Model

The Standard model of particle physics identifies 17 unique elementary particles, shown in figure 1, split into two general groups, fermions which are the building blocks of matter and bosons describing the interactions between particles.

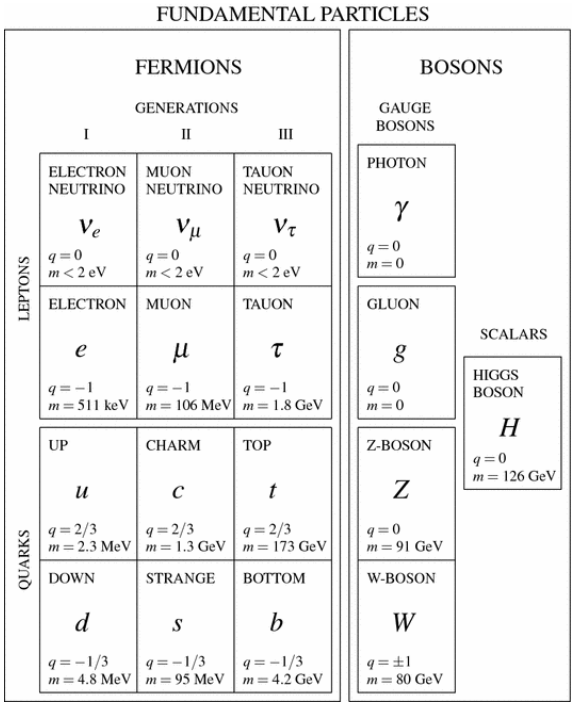

Figure 1: Standard model of particle physics with q being the electric charge and m the rest energy of the particles. Taken from[1].

Fermions are classified into quarks and leptons, each appearing in three generations with distinct charge and mass. Every fermion has a corresponding antiparticle with the same mass but opposite charge. Quarks q interact via all four fundamental

forces. Up-type quarks (u, c, t) have an electric charge of $+2/3$, while down-type quarks (d, s, b) carry $-1/3$. They also possess one of three color charges (red, green, or blue), enabling strong interactions. Antiquarks $\bar{q}$ carry corresponding anticolors. Leptons, unlike quarks, lack color charge and do not experience strong interactions. The charged leptons—electron e, muon μ and tau τ—interact electromagnetically and weakly. Neutrinos $(\nu_e, \nu_\mu, \nu_\tau)$ have no charge and interact only via the weak force. Bosons are categorized as gauge bosons, which mediate fundamental forces, and the Higgs boson, which imparts mass to other particles. The photon γ mediates electromagnetism, the $W^\pm$ and Z bosons govern the weak force, and gluons g drive the strong interaction. Unlike photons, gluons carry color charge and can interact with themselves.

Two or more quarks held together by the strong interaction force are called hadrons. They can be divided into two broad families: baryons, made up of an odd number of quarks, and mesons, made of an even number of quarks. Additionally mesons are always made up of the same amount of quarks and anti-quarks. Below we will describe the particles of particular interest for this thesis, namely the Kaon, Pion, Lambda baryon, Phi meson and proton, with a special emphasis on their strangeness.

The Kaon K is composed of a quark-antiquark-pair and is with that a meson. The pair is made up of a light u- or d-Quark and a heavier strange Quark. Four different kinds of Kaons can be formed from these three quarks and their associated antiquarks, these are shown in table 1.

Table 1: Kaon

	K-anti-meson		K-meson	
	K^-	$\bar{K}^0$	K^0	K^+
quark-composition	$\bar{u}$	$\bar{d}$	d	u
	s	s	$\bar{s}$	$\bar{s}$
strangeness S	-1		1	

The Pion π is also a meson, it is composed of one up and one down quark. There are three different types of Pions, their compositions are shown in table 2.

Table 2: Pion

	π^+	π^0	π^-
quark-composition	$u\bar{d}$	$\frac{u\bar{u}-d\bar{d}}{\sqrt{2}}$	$\bar{u}d$
strangeness S	0		

The Lambda baryon Λ is, as the name suggests, a baryon, it is made up of one

up, one down and a third quark from a higher generation. With this there are four different Lambda baryons, their compositions are shown in table 3. In this thesis Λ^0 will be abbreviated with Λ.

Table 3: Lambda baryon

	Λ^0	Λ_c^+	Λ_b^0
quark-composition	uds	udc	udb
strangeness S	-1	0	

The Phi meson Φ is composed of a strange and antistrange quark and has strangeness zero. Lastly the proton p is a baryon made up of two up and one down quark and also has strangeness zero. Further information on these particles can be found in the Particle Listings of the Particle Data Group [2].

2.2 Quantum Chromodynamics

Quantum Chromodynamics (QCD) is the fundamental theory of strong interactions between quarks mediated by gluons. These interactions are determined by the color charge of the quarks in each interaction.

The development of QCD started when the idea that hadrons are made up of more fundamental particles was first proposed in 1964 by Gell-Mann[3] and Zweig. The same year Oscar W. Greenberg introduced color as a three-valued charge degree of freedom. Color as a gauge symmetry was introduced by Yoichiro Nambu and by Moo Young Han and Yoichiro Nambu in 1965[4]. 1969 the existence of partons, i.e. parts of hadrons, was verified in the deep inelastic scattering of electrons on protons at the Stanford Linear Accelerator Center (SLAC). In 1973 asymptotic freedom, the property that the interaction between particles becomes weaker at shorter distances, was discovered by D. Gross and F. Wilczek[5], and independently by David Politzer[6] in the same year. Asymptotic freedom conversely also leads to a growing interaction between two strongly interacting particles at greater distances. This growing interaction can be exemplified by an elastic string. If you pull both ends apart more and more energy is deposited in the string and if the energy is too great the string will break into two. The same happens with quarks, but at the breaking point there is sufficient energy inside the field between the quarks to create a new quark, anti-quark pair. Figure 2 shows the particle production in the Color-Flux-Tube Model, which describes the string as a tube like confined region of force-carrying fields, but the model will not be further discussed here. This spontaneous production of quarks leads to the phenomenon that color charged particles can not be separated, i.e., color-confinement.

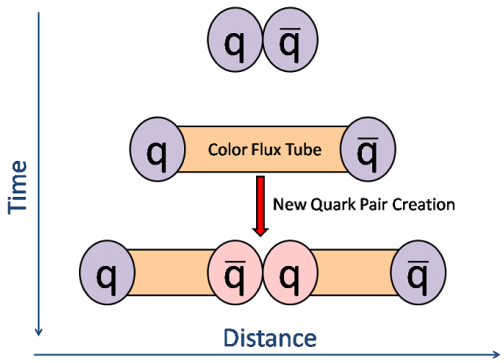

Figure 2: Particle production through string fragmentation inside the Color-Flux-Tube Model, taken from [7]

Although this picture of color-confinement "is supported strongly by the numerical calculations[...], at the moment there is no analytic approach or approximation that describes the behavior of QCD at large distances" [8]. Without this we are lacking a full descriptions of the strong interaction of particles. The Clay Mathematics Institute of Cambridge even included "Yang-Mills Existence and the mass gap" as one of its seven millennium problems, each allocated with a prize money of 1 M Dollar[9]. A solution to this problem would be a big step into proving color-confinement in QCD[10].
In the context of relativistic heavy-Ion collisions QCD can only be used to describe sub-processes or to deliver an input for modeling since a complete description of a collision based exclusively on first principles is impossible in practice.

2.3 Quark-Gluon-Plasma

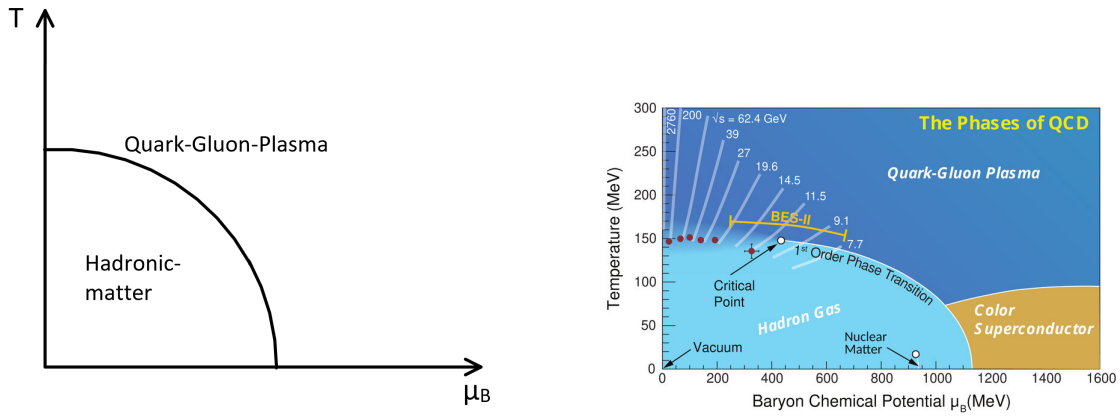

(a) by Cabibbo and Parisi in 1975 **(b)** conjectured as of 2024[11]

Figure 3: Phase Diagram of strongly interacting matter

Through the asymptotic freedom of particles QCD predicts a phase transition at

high temperature and/or increasing density where quarks and gluons gain absolute freedom. In such a state the color-confinement of quarks would be broken, i.e., quarks and gluons flow independently and ordinary hadrons do not exist anymore. In 1975 Cabibbo and Parisi identified the limiting temperature for this phase transition as the Hagedorn temperature, named after Rolf Hagedorn who had the idea that hadronic matter has a "melting point" in the 1960s[12]. They also sketched the first phase diagram of strongly interacting matter, see figure 3a. In the same year Collins and Perry argued that "superdense matter (found in neutron star cores, exploding black holes, and the early big-bang universe) consists of quarks rather than of hadrons"[13]. On February 10, 2000, CERN presented it evidence for "a new state of matter" and Professor Luciano Maiani, CERN Director General, said "The combined data coming from the seven experiments on CERN's Heavy Ion programs have given a clear picture of a new state of matter. This result verifies an important prediction of the present theory of fundamental forces between quarks. It is also an important step forward in the understanding of the early evolution of the universe. We now have evidence of a new state of matter where quarks and gluons are not confined."[14]. Although this state of matter can not be directly observed it's effects such as the absorption of jets and high level of thermalization can be studied.

The general idea of the phase Diagram of strongly interacting matter has since proven to be correct, but a lot of nuances of the transition have been found. After being revised and changed quite a lot over the last four decades figure 3b shows one of the latest iterations of the phase diagram by Toshihiro Nonaka.

2.4 Phases of Relativistic nucleus-nucleus Collisions

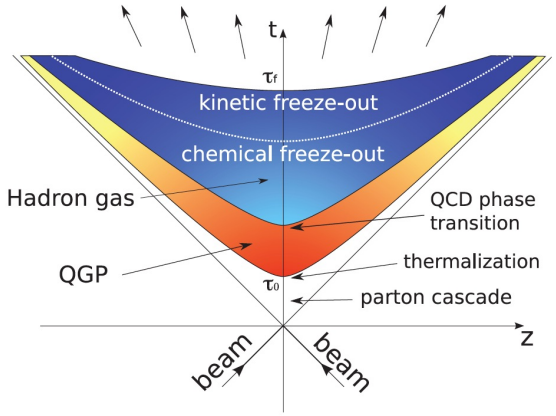

Figure 4: The space-time evolution of heavy Ion collisions [15]

In relativistic Heavy-Ion collisions the conditions, as shown in figure 3b, for the creation of QGP can be fulfilled. Figure 4 shows the evolution of the QGP in several

phases with four important phase transitions, namely thermalization, reconfinement, chemical and thermal freeze-out. Otherwise
Thermalization describes the evolution of the two nuclei into QGP. This strong interacting system then expands over time, therefore its density decreases and temperature drops. This leads first to the reconfinement of the Quarks and Gluons. This process is not instant and as such one may consider three phases in the reconfinement process, first to a good approximation the matter is an expanding quark-gluon plasma, later it is a mix of plasma and hadron gas and finally it becomes a pure hadron gas. The system keeps expanding and cooling, while the composition is still able to change through inelastic hadron collisions. The point where the chemical composition of the system stops changing is when inelastic scattering ceases. This is called the chemical freeze-out. Wether this point is the same for all particles or different freeze-out conditions exist for different particles is still a topic of research. With further expansion the density of the formed hadronic gas keeps decreasing and the mean free path of particles increases. Eventually this leads to the decoupling of hadrons from the system, i.e., collisions, and with that inelastic scattering, between the hadrons stop and they travel freely to the detectors. Since after that the momenta of the particles are fixed it is called the kinetic freeze-out. Just like the reconfinement the process of decoupling happens over time, e.g., particles may decouple at very high densities, if the expansion rate of the system is much larger than the scattering rate, and different types of particles may decouple at different times. To address the differing freeze-out points a hierarchy of different freeze-out points can be introduced to describe this complicated dynamic process [8], the usefulness of this approach for the chemical freeze-out in this case is discussed in section 8.

2.5 Theoretical models for relativistic nucleus-nucleus collisions

In central Au+Au collisions at the highest possible beam energies at RHIC ($\sqrt{s_{NN}} = 200$), a total charged particle multiplicity of approximately 5300 was achieved[8]. This means that the number of particles measured after the collision exceeds the number of particles in the beams by a factor of 10. Since the quantity of particles involved in these collisions can be very big theoretical models are used which describe large macroscopic systems, such as thermodynamics, hydrodynamics, kinetic gas theory, field theory at finite temperatures and densities, non-equilibrium field theory, as well as Monte Carlo simulations [8].
In general these models use simple thermodynamic or hydrodynamic concepts. Thus they can be divided into two groups, dependent on the concepts they are based on. Thermodynamic approaches are used to try to explain the relative abundance of

hadrons, i.e the ratios of hadron multiplicities, whereas hydro-inspired models focus on the analysis of the hadronic transverse-momentum spectra. The first group can also be subdivided into thermal and statistical models.
Using a few thermodynamic parameters, the thermal models usually do a very good job in describing the relative yields of many hadronic species at the chemical freeze-out. For example, within the grand canonical version of the thermal model many successful fits were obtained with only two independent parameters, T_{chem} and μ^{B}_{chem}, which are the values of the temperature and baryon chemical potential at the chemical freeze-out[8]. The exact implementation of this approach for the model used to calculate the theoretical data in this thesis is discussed in section 4.

3 Experimental approach

The data for this thesis encompasses a wide range of energies and stems from four different particle accelerators. These each provided the data for a certain energy regime:

2-6 GeV	Alternating Gradient Synchrotron (AGS) at Brookhaven National Laboratory
6-20 GeV	Super Proton Synchrotron (SPS)
20-200 GeV	Relativistic Heavy Ion Collider (RHIC) at Brookhaven National Laboratory
>200 GeV	Large Hadron Collider LHC at the "Conseil Européen pour la Recherche Nucléaire" (Cern)

All four particle accelerators are synchrotrons and their basic functionality is the same. They each consist of two independent, parallel rings in which positively charged particles are accelerated in bunches, these bunches are put behind each other with as little space as possible to form beams of particles. These beams move in opposite directions in the two rings, in one ring running clockwise and in the other anticlockwise, and are guided by strong magnets. In general, the bigger the circumference of the rings the higher the achievable maximum energy per beam, because the strength of the magnets which guide the beams are limited. A bigger radius lowers the bending radius of each individual magnet, although more are required, and with that increases the momentum at which circular motion of a particle can be maintained. To collide the beams in the two rings all synchrotrons have Interaction Points (IP), although their number varies. Around these IPs the particle detectors are constructed to measure the results of beam collisions.
The next subsections will look at two important descriptors of a collision, the centrality and the rapidity, with which the results can be characterized.

3.1 Centrality

The outcome of a collision depends among other things on the number of participating nucleons, as nuclei are extended objects a measure of how many nucleons of the colliding nucleus participate is needed. Figure 5 illustrates the collision of two nuclei. The distance between the centers of the two nuclei is given by the impact parameter b and the smaller this value the more nucleons collide. The centrality c is defined as a fraction of geometrical cross sections of the colliding nuclei:

$$c = \frac{\sigma(b)}{\sigma(b_{max})} = \frac{b^2}{4R_A^2}, \tag{1}$$

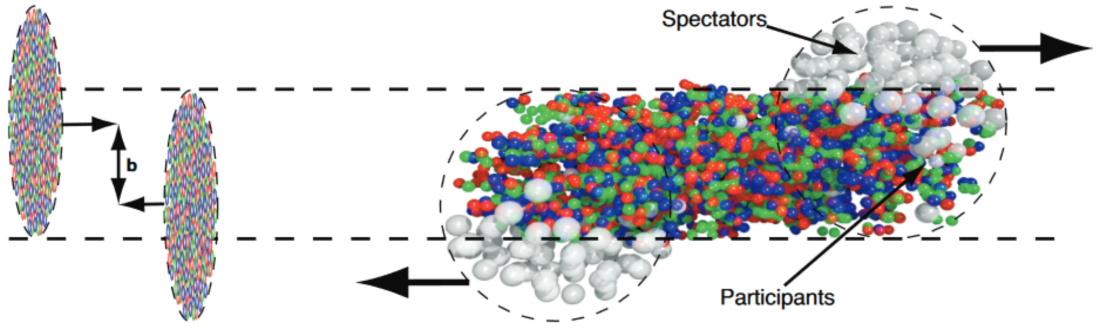

Figure 5: Collision between two ions viewed as disks, taken from [17].

with b being the impact parameter and R_A the nuclear radius of the colliding nuclei. Experimentally the impact parameter can not be observed directly, but central collisions have the most interacting particles and with that produce the most particles. With this the collisions with the highest number of measured charged particles, charged-particle multiplicity, are assigned to be the most central collisions, while collisions with low multiplicities are interpreted as peripheral[16].

3.2 Rapidity

Rapidity is used to express angles of a detected particle with respect to the axis of the colliding beams, depicted in figure 5 by the black arrows of the two disk pointing toward each other. It is defined as

$$y = \frac{1}{2} \ln \frac{\left(E + p_{||}\right)}{\left(E - p_{||}\right)} = \operatorname{arctanh}\left(\frac{p_{||}}{E}\right) = \operatorname{arctanh}\left(\frac{v_{||}}{c}\right), \tag{2}$$

where $p_{||}$ and $v_{||}$ are the components of the momentum and velocity parallel to the axis of the beam and $E = \sqrt{m^2 + \vec{p}^2}$, with the mass of the particle m and its momentum $\vec{p}$, is the total energy of a particle[8]. Rapidity has the value zero for particle trajectories that are perpendicular to the beam, and positive or negative values for those at an angle to the beam. The rapidity distribution of particle yields can roughly be described by rather broad Gaussians centered at zero[8]. With this background we can define yields at mid-rapidity as the number of particles traveling close to perpendicular to the beam axis.
In a similar way to the rapidity one can define the pseudorapidity variable η as:

$$\eta = \frac{1}{2} \ln \frac{\left(|\vec{p}| + p_{||}\right)}{\left(|\vec{p}| - p_{||}\right)} = \ln\left(\cot\frac{\theta}{2}\right) = -\ln\left(\tan\frac{\theta}{2}\right), \tag{3}$$

which has the advantage that the particle does not need to be known to calculate it[8]. This is of special interests for particles at mid- rapidity because in this region they are approximately equal, $y \approx \eta \approx 0$[8].

4 Model Description

This chapter goes over the general model used by A. Andronic to calculate the theoretical data used in this thesis. Specific assumptions and the implementation of the model for the theoretical data is explained in the next section.
The freeze-out is the process of thermalisation of the system after the collision. After this the system of hadrons has reached chemical and thermal equilibrium. We want a way to predict the microstate, a specific configuration of a system that describes the precise positions and momenta of all the individual particles or components that make up the system, of this system at thermodynamic (chemical and thermal) equilibrium.
In statistical mechanics there is a statistical ensemble that represents all possible states of a mechanical system in thermal equilibrium with a energy reservoir, the canonical ensemble. A given canonical ensemble is characterized by three constant variables, the number of particles N in the system, the systems volume V and the absolute temperature T. It assigns each distinct microstate a probability P, given by the function:

$$P = \exp\left(F - E\right)/(kT). \tag{4}$$

E is the total energy of the microstate, k is the Boltzmann constant and F is the Helmholtz free energy, which describes the thermodynamic potential of a closed system at a constant temperature. With this probability we can predict the microstates of the system at thermal equilibrium.
Since the possible states after freeze-out can differ in both their total energy and total number of particles, because they can be converted into each other, we need to generalize the canonical ensemble. The grand canonical ensemble is just that, a statistical ensemble which represents all possible states of a mechanical system in thermodynamic equilibrium with a energy/particle reservoir. The thermodynamic variables characterizing the grand canonical ensemble are chemical potential μ, absolute temperature T and the system's volume V. Analogous to the canonical ensemble the grand canonical ensemble represents all possible states by assigning each distinct microstate a probability given by the function:

$$P = \exp^{(\Omega+\mu N-E)/(kT)}. \tag{5}$$

Here N is the number of particles in the system, E is the total energy in the system, k is the Boltzmann constant and Ω is the grand potential. The grand potential is a constant of the system, which characterizes the system as a whole and is defined as:

$$\Omega(T, V, \mu) = F(T, V, N) - \mu N, \tag{6}$$

which is the Legendre transform of F, where the natural variable N is replaced by μ, [18] chapter 5.4. In case of s particles, which vary in number, the probability expression can be generalized to

$$P = \exp^{(\Omega+\mu_1 N_1+\mu_2 N_2+\cdots+\mu_s N_s-E)/(kT)} \tag{7}$$

Most thermodynamic variables can be expressed in terms of the partition function, a function which describes the statistical properties of a system in thermodynamic equilibrium, or its derivatives. As such for each particular statistical ensemble a partition function can be crafted which represents that ensemble. For the grand canonical ensemble the partition function is

$$Z = \exp^{-\Omega/(kT)}, \tag{8}$$

see [18] chapter 10.2, with this the probability can be rewritten as

$$P = \frac{1}{Z} \exp^{(\mu N-E)/(kT)}. \tag{9}$$

A statistical ensemble in quantum mechanics is represented by a density matrix, denoted by $\hat{p}$. With $E = \langle \hat{H} \rangle$, $N = \langle \hat{N} \rangle$ and $\beta = 1/kT$ the grand canonical density matrix is

$$\hat{p} = \frac{\exp^{-\beta(\hat{H}-\mu\hat{N})}}{Z}, \tag{10}$$

with the partition function

$$Z = Tr[\exp^{-\beta(\hat{H}-\mu\hat{N})}], \tag{11}$$

see [18] chapter 12.3. In general the chemical potential μ_i of strongly interacting matter can be described as a linear combination of the the baryon number μ_B, the strangeness μ_S, charm μ_C and isospin μ_{I_3}. These are treated as model parameters which control the net baryon number N_B, strangeness S, charmness C and total isospin I_3^{tot} of the system. The i-th hadron can thus be described through its baryon number B_i, strangeness S_i, charmness C_i and third component of the isospin I_{3i} [19]. With these we define the overall chemical potential of the i-th hadron as:

$$\mu_i = B_i\mu_B + S_i\mu_S + I_{3i}\mu_{I_3} + \mu_C C_i \tag{12}$$

The use of the chemical potentials μ_B, μ_S, μ_C and μ_Q allows for the satisfaction of the appropriate conservation laws. Assuming the matter at freeze-out originates from the initial nuclear matter of the two colliding nuclei the total strangeness and the ratio of the electric charge to the baryon number at freeze-out have to be the

same as the ones of the colliding nuclei, because particles can only be produced in particle anti-particle pairs [20]. Since the strangeness and charmness of a nucleus is zero the strangeness/charmness conservation can be written as:

$$\sum_i n_i(T, \mu_B, \mu_S, \mu_Q) S_i = Net\ S = 0, \tag{13}$$

$$\sum_i n_i(T, \mu_B, \mu_S, \mu_Q) C_i = Net\ C = 0. \tag{14}$$

For the total isospin and net baryon number ratio of the colliding nuclei, which are also conserved during the formation and subsequent evolution of the system created in RNNC, we can write their conservation through their ratio in the colliding nuclei:

$$R = \frac{Net\ I}{Net\ B} = \frac{I_3^{tot}}{N_B} \tag{15}$$

with that we get:

$$\sum_i n_i(T, \mu_B, \mu_S, \mu_{I_3}, \mu_C) I_{3i} = R \sum_i n_i(T \mu_B, \mu_S, \mu_Q) B_i. \tag{16}$$

The net baryon number and total isospin of the system need to be specified according to the colliding nuclei studied. "The degree of stopping of the colliding nuclei, which is energy dependent and cannot be precisely determined experimentally, brings some uncertainty in the choice of N_B and I_3^{tot}. In our case, as we study central collisions of heavy nuclei (Au or Pb), but focus on the data at mid-rapidity, we have chosen N_B=200 and I_3^{tot}=-20."[19] Using these values and all the conservation laws the produced matter may be characterized only through the baryon chemical potential μ_i and the absolute temperature T. The partition function in the grand canonical ensemble with these is written as:

$$Z^{GC}(T, V, \mu) = Tr\left[\mathrm{e}^{-\beta(\hat{H} - (B\mu_B + S\mu_S + I_3\mu_{I_3} + \mu_C C))}\right]. \tag{17}$$

The Hamiltonian in the partition function is usually taken such as to describe a hadron resonance gas because "it contains all relevant degrees off freedom of the confined, strongly interacting medium and implicitly includes interactions that result in resonance formation. Secondly, this model is consistent with the equation state obtained from LGT below the critical temperature"[21] The hadron mass spectrum contains all contributions from all hadrons listed in the Particle Data Group Particle Listings [2]. The grand potential of a hadron resonance gas can, if baryon number, strangeness, charm and isopsin conservation are included, be written as the sum of grand potentials of all particles of the hadron mass spectrum. With this we can rewrite the partition function in terms of all statistical ensembles of the individual

particles i:

$$\begin{aligned} Z(T,V,\mu) &= \mathrm{e}^{-\beta\Omega} \\ &= \mathrm{e}^{-\beta(\Omega_1+\Omega_2+\cdots)} \\ &= \prod_i \mathrm{e}^{-\beta\Omega_i} \\ &= \prod_i \mathrm{e}^{-\beta(E_i-(B_i\mu_B+S_i\mu_S+I_{3i}\mu_{I_3}+\mu_C)} \\ &= \prod_i \mathrm{e}^{-\beta(E_i-\mu_i)} \\ &= \prod_i Z_i(T,V,\mu_i) \end{aligned} \tag{18}$$

Here E_i is the total energy of a given particle i and μ_i its chemical potential. We see that the partition function is the product of all individual partition functions of the individual particles. With the normal logarithm we get:

$$\ln Z(T,V,\mu) = \sum_i \ln Z_i(T,V,\mu_i) \tag{19}$$

These individual partition functions for a species i with $\hbar = c = 1$ and a spin-isospin degeneracy factor $g_i = (2J_i + 1)$, where J_i is the total angular momentum quantum number of the particle, are defined as:

$$\ln Z_i = \frac{V\, g_i}{2\pi^2} \int_0^\infty \pm p^2 dp \ln\left[1 \pm \exp\left(-\beta(E_i - \mu_i)\right)\right], \tag{20}$$

from which the density is then calculated according to:

$$n_i = \frac{N_i}{V} = -\frac{T}{V}\frac{\partial \ln Z_i}{\partial \mu} = \frac{g_i}{2\pi^2}\int_0^\infty \frac{p^2 dp}{\exp[\beta(E_i - \mu_i)] \pm 1}. \tag{21}$$

The $(+)$ sign is for fermions and $(-)$ sign is for bosons. The total energy E_i can be expressed through the impulse and rest energy of the particle

$$E_i = \sqrt{p^2 + m_i^2}, \tag{22}$$

these rest energies being the nominal mass m_i from the Particle Listings [2] of the particle i. If the particle i has a finite width Γ_i the thermal yield of the particle is more appropriately obtained by weighting equation 21 over the range of masses to take the mass spread into account[22]. This is taken into account through an additional integration over the particle mass with a Breit-Wigner distribution:

$$n_i = \frac{g_i}{2\pi^2}\frac{1}{N_{BW}}\int_{M_0}^\infty dm \int_0^\infty \frac{\Gamma_i^2}{(m - m_i)^2 + \Gamma_i^2/4}\frac{p^2 dp}{\exp\left[\beta(E_i^m - \mu_i)\right] \pm 1}, \tag{23}$$

where N_{BW} is the normalization of the Breit-Wigner distribution and M_0 the threshold for the dominant decay channel[19]. Here the energy E_i has to be calculated for every value of m in the integration step, as such $E_i^m = \sqrt{p^2 + m^2}$ has to be used.
The interaction of the hadrons and resonances are included by implementing a hard core repulsion, i.e. a Van der Waals-type interaction. This is done by means of a excluded volume correction implemented in an iterative procedure according to ref. [23]:

$$P^{excel.}(T, \mu) = P^{id.gas}(T, \hat{\mu}); \qquad \hat{\mu} = \mu - V_{eigen} P^{excel.}(T, \mu). \tag{24}$$

V_{eigen} is calculated for a radius of 0.3 fm and is considered identical for all hadrons [24].
The model described so far is well suited for a system with a large number of produced hadrons, but for smaller systems, peripheral nucleus-nucleus collisions and for low energies, in case of strangeness production, a canonical ensemble treatment is mandatory[25], which leads to a phase reduction for particle production. This is called the "canonical suppression" and can be characterized through a strangeness suppression factor F_S. It gives, with a good approximation, a relation between the density calculated in the canonical approach, n_i^C, and the grand canonical approach, n_i^{GC}, as described above. For a particle with net strangeness S the relation has been shown [26] as: $n_i^C = n_i^{GC}/F_S$. The factor F_S is the ratio between the Bessel function of the order S, the net strangeness of the yield, and the Bessel function of the order 0:

$$F_S = \frac{I_0(x)}{I_S(x)}, \tag{25}$$

where the argument x of the Bessel function is defined as:

$$x = \sum_i n_i(T, V, \mu_i) \cdot V_C, \tag{26}$$

i.e. the total yield of all strange and antistrange hadrons. This factor is also dependent on the temperature T, energy $\sqrt{s_{NN}}$ and Volume V_C [27].
To obtain the particle yields from the densities n_i^{CG}, obtained through the partition function as described above, at a given temperature T, volume V and baryon chemical potential μ_B, one multiplies them with the volume V of the fireball [28]. Also, because the freeze-out conditions are universal, the yields are the same for all collisions and they can all be described as one big fireball, where the volume is the sum of the volume of all individual fireballs. To experimentally measure the yield of a singular collision, the total number of collisions or Luminosity of the accelerator has to be measured as well as the total yields. If one looks at ratios of particle yields, instead of individual particle yields, the volume, as it is the same for all densities, disappears as a parameter and with that T and μ_B are the only model parameters of

the particle ratio. In ratios with non zero net strangeness the strangeness suppression adds the additional parameter of the canonical Volume V_C. Also the number of collisions in the particle beam becomes totally irrelevant as the ratio is the same for all collisions and with that is also the same as the ratio of one big fireball.

5 Fits to experimental data

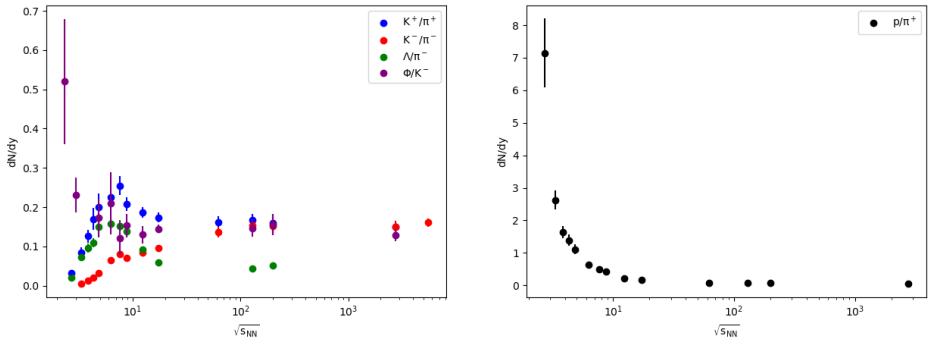

Figure 6: Energy dependence of the experimental hadron yields from central collisions at mid-rapidity for the five analyzed particle ratios.

The ratio yields for the five different ratios analyzed in this thesis were obtained from central collisions at mid-rapidity. To extract the best temperature T_I for the model we perform fits of the experimental data, shown in 6, with model calculations. The model data has been calculated based on the theoretical basis discussed in section 4. The temperature is defined as:

$$\frac{T}{k_B} = T_{cf} = \frac{T_{cf}^{lim}}{1 + \exp\left[a - \ln\left(\sqrt{s_{NN}}\right)/b\right]} [28], \tag{27}$$

with $\sqrt{s_{NN}}$ in GeV and T_{cf}^{lim}=154.8 MeV. T_{cf}^{lim} describes the upper bound which can be seen when looking at the energy dependency of the temperature, see figure 7a. This was established as the "line of chemical freeze-out"[21]. With different values for a and b four different temperature curves were created, see figure 7a, which will each be characterized through their value at $\sqrt{s_{NN}}$=2.7 GeV (T0: 63.8 GeV, T1: 74 GeV, T2: 83.6 GeV and T3: 92.6 GeV). For all temperatures the baryon chemical potential is defined through:

$$\mu_B = \frac{1307.5\,\text{MeV}}{1 + 0.288\sqrt{s_{NN}}} [28], \tag{28}$$

with $\sqrt{s_{NN}}$ in GeV, we get figure 7b. With temperature and baryon chemical potential determined the only free parameter for the model calculations of the four temperatures is the canonical volume. This parameter has been fitted by A. Andronic for for each temperature, with figure 8 showing the results of those fits. Because of the error on these values the model calculations are done for three different sets of Volumes: the ideal volume, V1, as determined by the fit, the upper limit of the

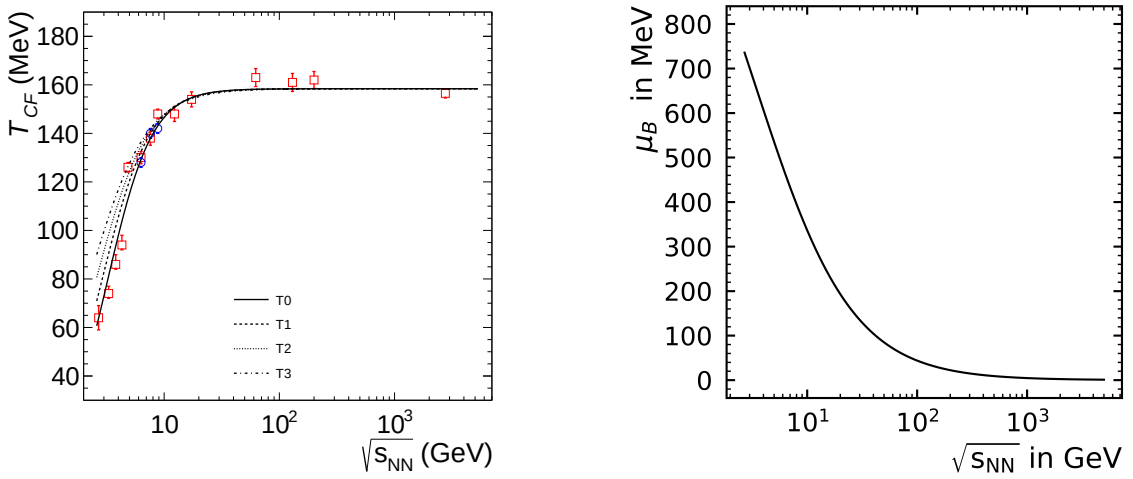

(a) Temperatures (T_{cf}=T/k_B)[27]

(b) Baryon chemical potential

Figure 7: Parameters T and μ_B used for model calculations

confidence interval of the volume, V2, and lower limit of the confidence interval of the volume, V3. Figure 13 shows all relevant theoretical Data below energies of

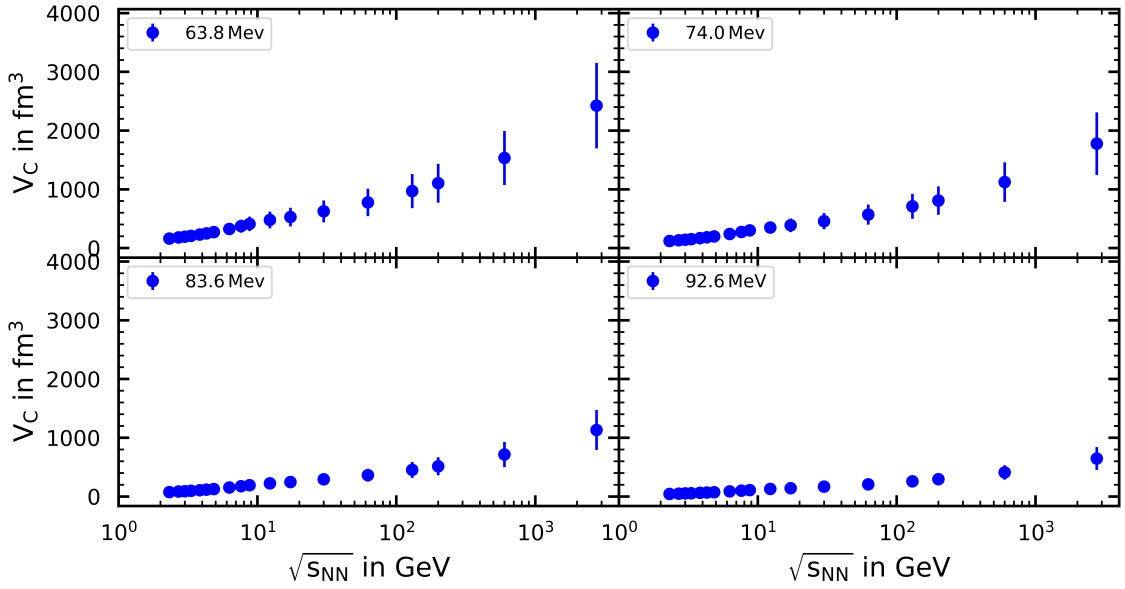

Figure 8: Volume dependent on particle energy for the four temperatures

$\sqrt{s_{NN}}$=10 GeV. The threshold is introduced because the chemical freeze-out temperature barely varies above it and we want to look specifically at the influence of the temperature. Each individual subfigure shows the experimental Data together with the corresponding theoretical graphs for the ideal volume and both ends of the confidence interval. Here especially the graphs of the ratio $\frac{p}{\pi^+}$ stick out as it has no uncertainty, that is because the net strangeness of the ratio is zero. Since the canonical volume is not a parameter for the calculation of that ratio the uncertainty

falls away.
The best fit is obtained by minimizing the χ^2 distribution. χ^2 is defined as:

$$\chi^2 = \sum_i \frac{(R_i^{exp} - R_i^{mod})^2}{\sigma^2}, \tag{29}$$

where R_i^{exp} is the measured value of the ratio of hadron yields, σ_i is the corresponding experimental error and R_i^{mod} the value from the model calculations. The experimental error is sum of the squares of the statistical and systematic error

$$\sigma = \sqrt{(\Delta f_{statistical})^2 + (\Delta f_{systematic})^2}. \tag{30}$$

These values of χ^2 are plotted dependent on their characterizing temperature and a parabolic χ^2 distribution is assumed. To find the parameters of the parabola the least squares method as described in section 6.5 is used. The ideal temperature which characterizes the best fit at $\sqrt{s_{NN}}$=2.7 GeV, in the same way as T0, T1, T2 and T3 characterize the temperature graphs of the theoretical data, is the minimum of the fitted parabolic function. The uncertainty of the ideal temperature can be approximated with:

$$\Delta T = \pm[T(\chi^2_{min} + 1) - T(\chi^2_{min})], \tag{31}$$

where χ^2_{min} is the value of χ^2 at T_I [27]. Lastly to evaluate how good the result of the best fit is we will look at χ^2/dof, where dof is defined as:

$$dof = N_i - N_{parameters}, \tag{32}$$

with N_i being the number of data points and $N_{parameters}$ the number of free parameters which are fitted. In our case the only free parameter is the temperature so $N_{parameters} = 1$.

6 Least squares

The following section is based on the book "Applied linear algebra and matrix methods" by Timothy G. Feemann [29]. It will show a basic way to find a solution to the least squares problem, which can be summarized as follows:

> Given a Matrix, $A \in \mathbb{R}^{n \times m}$ and a Vector, $b \in \mathbb{R}^n$. Over all choices of $m \times 1$ vectors $\mathbf{x}$, minimize the mismatch between $A\mathbf{x}$ and $\mathbf{b}$ (i.e., pick $\mathbf{x} \in \mathbb{R}^m$ to make $A\mathbf{x}$ as much like $\mathbf{b}$ as possible).

$$\min_{\mathbf{x} \in \mathbb{R}^m} \|A\mathbf{x} - \mathbf{b}\| \tag{33}$$

As well as how to use this knowledge for curve fitting. For this we will first go over a few basics which are needed to solve the problem.

6.1 Angle between two vectors

For two nonzero vectors $\mathbf{a}$ and $\mathbf{b}$ in $\mathbb{R}^N$, the angle θ between them is the angle between 0 and π radians whose cosine is given by

$$\cos(\theta) = \frac{a_1 b_1 + a_2 b_2 + \cdots + a_N b_N}{\|\mathbf{a}\| \|\mathbf{b}\|}. \tag{34}$$

6.2 Inner Product

For two vectors $\mathbf{a}$ and $\mathbf{b}$, both in $\mathbb{R}^N$, the expression $\mathbf{a}^T\mathbf{b}$ is defined as

$$\mathbf{a}^T\mathbf{b} = \begin{bmatrix} a_1 & a_2 & \cdots & a_N \end{bmatrix} \cdot \begin{bmatrix} b_1 \\ b_2 \\ \vdots \\ b_N \end{bmatrix} = a_1 b_1 + a_2 b_2 + \cdots + a_N b_N. \tag{35}$$

The resulting Scalar is called the *inner product* of $\mathbf{a}$ and $\mathbf{b}$.
Note that $\mathbf{b}^T\mathbf{a} = \mathbf{a}^T\mathbf{b}$.
With this Definition in mind we can rewrite the formula from 6.1 to

$$\cos(\theta) = \frac{\mathbf{a}^T\mathbf{b}}{\|\mathbf{a}\| \|\mathbf{b}\|}. \tag{36}$$

Note that if the inner product is equal to zero the right side is zero and θ is subsequently equal to 90°.

6.3 Column space of a Matrix

This subsection is based on chapter 5.1 of the book[29]. A system of M linear equations with N unknowns can be represented in matrix form as $Ax = b$, where:

- A is an $M \times N$ matrix of coefficients, denoted by $A = [a_{i,j}]$, where $a_{i,j}$ represents the element in the i-th row and j-th column of the matrix.
- $x = [x_1, x_2, \ldots, x_N]^T$ is the unknown vector in $\mathbb{R}^N$, which contains the variables $x_1, x_2, \ldots, x_N$.
- $b = [b_1, b_2, \ldots, b_M]^T$ is a given vector in $\mathbb{R}^M$, representing the constants on the right-hand side of the system of equations.

The left-hand side Ax can also be interpreted as a sum of numerical multiples of the column vectors of A. Specifically, if A is written as:

$$A = \begin{bmatrix} | & | & \ldots & | \\ a_1 & a_2 & \ldots & a_N \\ | & | & \ldots & | \end{bmatrix} \tag{37}$$

where each column a_j is a column vector in $\mathbb{R}^M$, the product Ax can be expanded as:

$$Ax = x_1 a_1 + x_2 a_2 + \cdots + x_N a_N \tag{38}$$

This means that the vector Ax is a linear combination of the columns of A, with the scalar coefficients being the corresponding components of the vector x.

In other words, each component of the vector b, represented as b_i for $i = 1, 2, \ldots, M$, is a result of the combination of the coefficients $a_{i,j}$ from matrix A, weighted by the unknowns x_j. Therefore, the system of equations describes how the vector b can be obtained by linearly combining the column vectors of A using the unknowns in the vector x.

A solution to $Ax = b$ are the specific values of x that result in a true equation. This is only possible if the right hand side b is a linear combination of the column vectors of A. In other words b has to be part of the column space Col(A), i.e. the span of the collection of the column vectors, and conversely the column space is the set of all vectors b for which the system $Ax = b$ has a solution.

6.4 Least squares

This subsection is based on chapter 5.2 of the book[29]. Suppose we have a system as described in 6.3 and b is a vector in $\mathbb{R}^M$, but not in $Col(A)$. Thus, the system $Ax = b$ does not have a solution, otherwise the solution be calculated directly and no minimization would be needed.
To approximately solve the system, we look for a vector $\hat{x}$ such that $A\hat{x}$ is closest to b among all vectors in $Col(A)$. That is, we wish to find a vector $\hat{x} \in \mathbb{R}^N$ such that

$$\|Ax - b\| = \min_{x \in \mathbb{R}^N} \|Ax - b\|. \tag{39}$$

This is the least squares problem as described in the beginning. A vector $\hat{x}$ that satisfies the equation 39 is called a least squares solution to the problem.

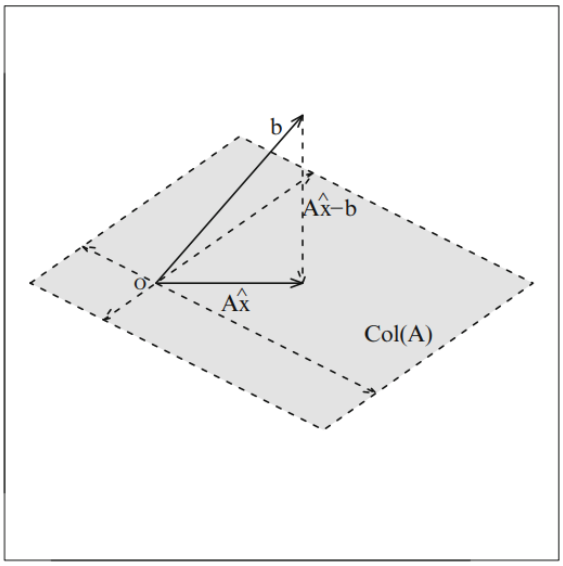

Figure 9: For b not in $Col(A)$, a least squares solution $\hat{x}$ has the property that $A\hat{x} - b$ is orthogonal to $Col(A)$.[30]

Geometrically, the vector $A\hat{x}$ is the projection of the vector b onto the column space of A. The difference $A\hat{x} - b$, which represents the "error" or the vector of residuals, must be orthogonal to the column space of A. That way, we have a right triangle with b as its hypotenuse and the vectors $A\hat{x}$ and $(A\hat{x} - b)$ as the adjacent sides, see figure 9. This ensures that $A\hat{x}$ is the closest point to b in $Col(A)$. Since the difference vector $A\hat{x} - b$ is orthogonal to the column space of A, it must have an inner product 6.2 of zero with every column vector a_j of the matrix A.

$$a_j^T(A\hat{x} - b) = 0 \tag{40}$$

This condition can be rewritten in matrix form and we obtain the following matrix equation:

$$A^T(A\hat{x} - b) = 0. \tag{41}$$

This equation represents the condition for $\hat{x}$ to be the least squares solution to the problem and can be expanded to:

$$A^T A\hat{x} = A^T b. \tag{42}$$

This is known as the **normal equation**. It is a key result in the least squares problem, as it provides a way to solve for the vector $\hat{x}$ that minimizes the squared error $\|A\hat{x} - b\|^2$. In practice, solving the normal equation allows us to find the best approximation of b within the column space of A.

6.5 Multiple Linear Regression

This subsection is based on chapter 5.3.1 of the book [29]. Suppose we have N input variables $X_1, X_2, ..., X_N$ and an output variable Y, and we suspect that there my be a linear relationship between them of the form

$$\beta_0 + \beta_1 X_1 + \beta_2 X_2 + \cdots + \beta_N X_N \approx Y, \tag{43}$$

where the parameters β_i are constants which we want to determine. With a sample of M observations, where each observation includes measurements of all the input variables along with the output variable, we can write the i-th observation as

$$\beta_0 + \beta_1 x_{i,1} + \beta_2 x_{i,2} + \cdots + \beta_N x_{i,N} \approx y_i. \tag{44}$$

Here the i-th measurement of the j-th input variable X_j is denoted by $x_{i,j}$ and the corresponding i-th measurement of Y by y_i. To express this in matrix form we set the output as a vector y, and take x_j to be the column vector of measured values of the variable X_j where X_j with $j \in [1, \cdots, N]$ are the column vectors of A. When the parameters β_i are also expressed as vector β we get

$$A = \begin{bmatrix} 1_M & X_1 & \cdots & X_N \end{bmatrix}, \quad \boldsymbol{\beta} = \begin{bmatrix} \beta_0 \\ \beta_1 \\ \vdots \\ \beta_N \end{bmatrix} \text{ and } \quad \boldsymbol{y} = \begin{bmatrix} y_0 \\ y_1 \\ \vdots \\ y_M \end{bmatrix}. \tag{45}$$

The conjecture is that $A\beta \approx \boldsymbol{y}$. The least squares solution is a vector $\hat{\beta}$ that satisfies the normal equation 42:

$$A^T A\hat{\beta} = A^T y. \tag{46}$$

To assess how well the model explains the data from the sample we compare the error $\|A\hat{\beta}-y\|$, which represents the difference between the predicted values $A\hat{\beta}$ and the observed values y, to the overall variability in y without considering the input variables X_j. If this error from the estimation is not significantly smaller than the intrinsic variability in y, the regression model does not provide much value. The total variability in a given sample is the sum of the squared differences between each observed value and the mean. The mean is defined as

$$\bar{y} = \frac{y_1 + \cdots + y_M}{M}. \tag{47}$$

With that the sum of the squared differences or total sum of squares (TSS) is defined as

$$TSS = (y_1 - \bar{y})^2 + \cdots + (y_M - \bar{y})^2 = \|y - \bar{y}\|^2. \tag{48}$$

Statisticians use a metric called R^2 to compare TSS with the sum of squared errors (SSE) resulting from the least squares solution, which is defined as

$$R^2 = 1 - \frac{SSE}{TSS} = \frac{\|A\hat{\beta} - y\|^2}{\|y - \bar{y}\|^2} \tag{49}$$

If regression estimates are perfect, then $R^2 = 1$. If the regression errors are large, then R^2 will be close to 0.

7 Program structure

The program works in four major steps: read files, filter data, calculate error and fitting, which are executed in series. Exactly one experimental dataset is required while the number of theoretical Datasets can be varied as desired. The Name of the input files is irrelevant, since they will be accessed through their file paths, but they have to be CSV-files. These input files are described in more detail in the next subsection. Each Function in the program will be performed independently from others, and the output should be stored in a designated variable for ease of use later.

7.1 Input files

As stated before the inputs have to be CSV-files, but the separator, right now designated as double spaces, can be swapped. The amount and order of the columns in the files are fixed. Although the columns do not need to be named the order of columns should be the same as the formats described below.
For the experimental data the current format is

$$\sqrt{s_{NN}} \quad \texttt{ratio} \quad \texttt{uncertainty}$$

where:

$\sqrt{s_{NN}}$	— energy per particle in the particle beam in GeV,
ratio	— ratio at the given energy,
uncertainty	— uncertainty of the given ratio

and for the theoretical data the current format is

$$\sqrt{s_{NN}} \quad \texttt{V1} \quad \texttt{V2} \quad \texttt{V3}$$

where:

$\sqrt{s_{NN}}$ — energy per particle in the particle beam in GeV,

V1 — ratio at the given energy and a given Volume V,

V2 — ratio at the given energy and the upper end of the confidence interval of the volume (V+ΔV)

V3 — ratio at the given energy and the lower end of the confidence interval of the Volume (V-ΔV).

From now on we will refer to the contents of one such file as a set, which corresponds to the data of a given temperature and ratio for all energies. Furthermore a ratio-set is all sets through all temperatures of a given ratio and a temperature-set is a all sets of a given temperature.

7.2 Read files

This step just takes the data of all input files and puts them in two dictionaries, one for the experimental data and one for the theoretical data. For that it is important that they are grouped correctly and there is the same order of ratios in every group. First the names of the ratios are listed, this also determines the order of the ratios in each group. The groups are the experimental sets and the individual temperature-sets, each group consists of the list of paths which refer to the individual input files, which are ordered after the order of the list of ratio names. Lastly the temperature-sets also each receive a name through a list. Lastly the groups of temperature-sets are put into a list, which has the same order as the names list.
The two dictionaries that are created have the names data_E, for the experimental data, and data_T, for the theoretical data.

7.3 Filter data

This step has three individual Functions:

energy_limits — energy per particle in the particle beam in GeV limited by lower and upper bonds

targeted_energy_limits — energy per particle in the particle beam in GeV limited by lower and upper bonds for a given ratio

get_theoretical_values — match theoretical data of all temperature-sets to the energies present in the experimental data

The inputs for the functions are as follows:

energy_limits (experimental data set, lower bound, upper bound)

targeted_energy_limits (experimental data set, ratio(s), lower bound, upper bound)

get_theoretical_values (experimental data, correct_p2pip)

energy_limits filters out all data which is not inside the bounds and gives out a new data set. targeted_energy_limits functions the same way but the bound is only applied to a given ratio or a list of ratios. Both Functions can be used in succession as often as ones wants and if one inputs contradictory bounds a whole ratio can be excluded.
get_theoretical_values filters all temperature-sets in data_T such that only ratios with energy values remain that correspond to ones in the experimental set. If theoretical values in any temperature-set are missing the temperature-set, ratio and energy of the missing value are printed into the console. If there are no missing theoretical values the statement: "The experimental data has corresponding theoretical

data for all temperatures." is printed. Only then can the filtered theoretical data be used in the calculate error functions! This function also has a second option (input is a boolean, default is False) which specifically corrects an error in the ratio-set p/π^+ of the here given theoretical data, where the values for the ends of the confidence interval of the volume are very outlandish, even though they should be the same as the ones of the mean volume. If this option is True the ratios of the mean volume will be used for all three columns

7.4 Calculate error

For this step there are five Functions:

error_extensive — calculates χ^2 with equation 7

error_E — sums χ^2 over all energies

error_E_dof — sums χ^2 over all energies and divides it by the degrees of freedom

error_ER — sums χ^2 over all energies and ratios

error_ER_dof — sums χ^2 over all energies and ratios and divides it by the degrees of freedom

The inputs for the functions are as follows:

error_extensive (experimental data, theoretical data)

error_E (experimental data, theoretical data)

error_E_dof (experimental data, theoretical data, parameters)

error_ER (experimental data, theoretical data)

error_ER_dof (experimental data, theoretical data, parameters)

All Functions only work when there is the same number of energy values per ratio in each temperature-set as in the experimental set. This is achieved with get_theoretical_values function from section 7.3, so that Function has to be used first and its output is the input for these Functions. The output of error_extensive is in the same format as the theoretical data it was generated from. error_E sums the values from error_extensive over all energies and outputs three error values in a List for every ratio of every temperature. The first value of the List is the error of V1, the second the error of V2 and the third the error of V3. Lastly error_ER sums the values from error_extensive over all energies and outputs three error values in a list for every temperature. The list has the same structure as the ones from error_E. For error_E and error_ER there is also a corresponding function which calculates χ^2/dof, with dof as defined in 5. The output has the same form as the two original functions, but to calculate dof a third input is needed which is the amount of free parameters.

All five functions also exist for δ^2 as error_delta_extensiv, error_delta_E, error_delta_E_dof, error_delta_ER and error_delta_ER_dof with exactly the same properties as the ones for χ^2. The Formula for δ^2 is

$$\delta^2 = \frac{(R^{exp} - R^{theo})^2}{(R^{exp})^2} \tag{50}$$

7.5 Fitting

For this step there are three Functions:

temperature_analysis — creates a parabolic fit dependent on temperature

temperature_analysis_ratios — creates a parabolic fit dependent on temperature for each ratio individually

plot_ideal_temperature — plots the ideal temperatures with their uncertainties

The inputs for the functions are as follows:

temperature_analysis (error data, temperatures, initial guess, show, dof)

temperature_analysis_ratios (error data, temperatures, initial guess, show, dof)

plot_ideal_temperature (ideal temperatures of ratios, ideal temperature)

temperature_analysis takes the error summed over the energies and ratios as input, as such any output of error_E, error_E_dof or its counterparts for δ^2 can be used as input. After that the temperatures of the individual temperature-sets have to be provided as a list of real numbers with the same order as the list of names of the temperature-sets. Lastly an initial guess has to be given. This is also a list of real numbers. The first number is the ideal temperature with the smallest error, the second number is the value of the smallest error and the third is the steepness of the curve. In other words the first two values are describing the position of the vertex and the third is the value of a of a parabolic function:

$$f(x) = ax^2 + bx + c. \tag{51}$$

After that are two optional inputs "dof" and "show". "dof" is for the naming of the y axis. If it is set to false it will just be χ^2 and if true χ^2/dof, this should be set according to the input error data. The default value of dof is False. "show" determines if the plot should be displayed, the default is True. The coordinates of the vertex of the fitted function and the uncertainty of the ideal temperature are printed in the terminal.
temperature_analysis_ratios has the same inputs but the inputs for "temperatures"

and ”initial guess” have to be modified such that they are a list of lists, where the first list is for the first ratio, the second for the second ratio and so on. The length of these lists naturally has to be the same as the amount of ratios. Each individual list for a given ratio is formulated the same as the ones for temperature_analysis, they are just grouped into one big list for the input. ”dof” and ”show” work just like they do for temperature_analysis. The coordinates of the vertices of the fitted functions and the uncertainties of the ideal temperatures are printed in the terminal.
Both temperature_analysis and temperature_analysis_ratios also output their calculated ideal temperatures with their corresponding uncertainties as lists. These lists are the inputs for plot_ideal_temperature. The optional input ”show” in the previous functions is exactly to suppress the display of the plots until all three are created, so that one can look at them all at the same time.

8 Results

Before looking at the temperature we will first talk about the influence of the canonical Volume on the model data. For higher energies the suppression factor and with that the influence of the canonical volume on the error of the model calculations decreases as the hadron multiplicity increases and the system becomes big enough to warrant a grand canonical approach. This energy dependence can be seen in figure 14 through the shrinking differences between the errors of the mean and the bounds of the confidence interval of the volume, because even though the standard deviation gets bigger, see figure 8, these have shrinking influence on the error. Looking only at the errors of energies below 10 GeV all ratios seem to additionally show the tendency that throughout the different temperatures the influence of the suppression factor scales with the observed error.

For Λ/π^- the error seems to grow continuously with higher temperatures and with growing temperature the difference between the error of the different volumes increases, even though there is no big difference between the standard deviations at these small energies, insinuating a growing influence of the canonical volume. Although Φ/K^- has the opposite tendency, lower error with higher temperatures, the influence of the suppression factor scales with the error. The only exception is the lowest energy of K^+/π^+, where it seems to be low even though the error is high. The ability of the volume to offset error this strongly could indicate an elliptical contour plot of temperature and volume, where small changes in volume have a big impact, but changes in temperature can be offset through the volume.

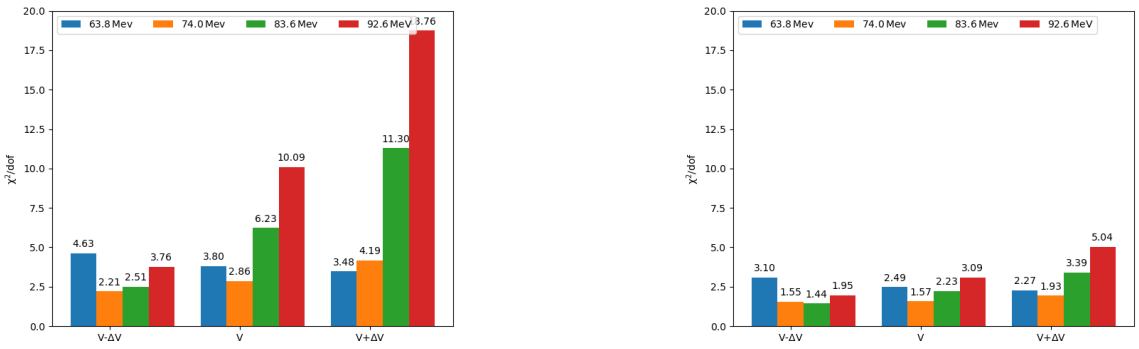

(a) All ratios and energies **(b)** Without Λ/π^-

Figure 10: Error dependent on Temperature and Volume

Figure 10a shows χ^2 added over all energies and ratios and it becomes apparent that the lowest volume almost universally gives a better description of the experimental data. Only for 63.8 MeV does the highest volume have the best agreement with the data. This shows again how tight the cone of agreement is for the volume.

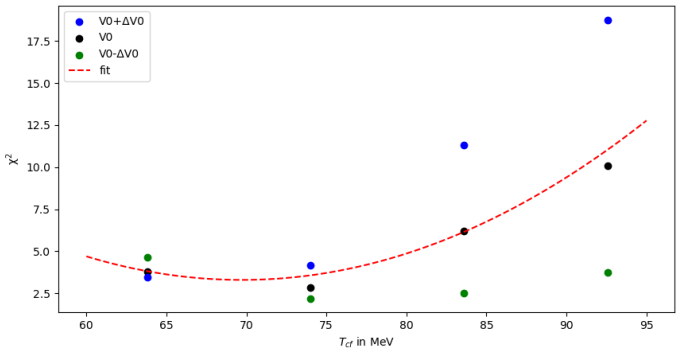

Figure 11: χ^2 distribution of energies below 10 GeV

Looking at Fig. 15 we can see that the biggest errors coincide with the errors of Λ/π^- and if we exclude this ratio from the sum, see figure 10b, we get drastically lower χ^2 values, but the trend of growing χ^2 with higher temperatures remains. The comparatively giant χ^2 of this ratio, and those few points more specifically, is because of the small error of the experimental data at those energies, which can't even be shown in figure 6. Because of that a small deviation from the experimental data leads to big values of χ^2. The χ^2 distribution of all volumes together is shown in figure 11. From it we get $T_{cf} = 69.72 \pm 1.37\,\text{MeV}$, with χ^2/dof =118.82/36. Although the error of the temperature is very low, the quality of the fit is not very good. Fitting each volume individually we get a much better result with V3, the outcome of all fits is summarized in Table 4.

Table 4: Summary of the results of the fits for different volumes

fitted volumes	T (MeV)	ΔT (MeV)	χ^2/N_{df}
V1 & V2 & V3	69.72	1.37	118.82/36
V1	69.99	1.41	112.12/36
V2	64.77	1.17	115.91/36
V3	79.47	1.67	76.16/36

While the fit is better it is still not very good, also the error on the temperature increased marginally, but is still very small. Additionally we can see a trend in the results in table 4, with shrinking volume the fit quality increases, but the error increases as well. If this trend continues good results might be achieved with even smaller volumes. It is important to note that this trend is happening because the smaller volumes disproportionally affect the higher temperatures and if we look at the ideal temperatures of the individual ratios for V3, see figure 12, it is clear that only ratios with strangeness suppression have such high ideal temperatures.

This implies at least a double kinetic freeze-out scenario, with different freeze-out temperatures for strange and non strange particles. This scenario is consistent with [31, 32]. With this we get an ideal temperature of 80.21 ± 1.69 MeV for the strange particles, which is practically the same as the one with all ratios because we only looked at one non strange ratios. Although the quality of the fit is slightly worse, see table 5, the fit for the non strange ratio is very good. The ideal temperature for non strange particles is equivalent with the ideal temperature of 54.72 ± 9.77 MeV form the p/π^+ particle ratio. As stated before this particular fit is very good, but a sample size of one is meaningless and other particle ratios need to be added. Fitting the

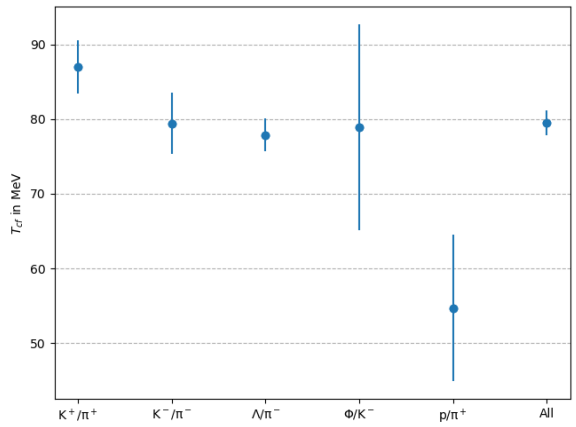

Figure 12: Ideal temperature of the individual ratios at the smallest volume

ratios individually has varying success, see table 5. Except for K^-/π^- and Λ/π^- the individual fits are really good. Even K^-/π^- is manageable, but Λ/π^- has such big values for χ^2 at lower energies, because of reasons discussed above, that the results are not very good. The very similar ideal temperatures for the different strange particle ratios make a multi stage freeze-out very unlikely, but a triple freeze-out, as described in [33], can not be excluded, because only single strangeness ratios were looked at.

Table 5: Summary of the results of the fits for different ratios at volume V3

fitted ratios	T (MeV)	ΔT (MeV)	χ^2/N_{df}
K^+/π^+	86.95	3.54	3.28/7
K^-/π^-	79.41	4.12	16.5/6
Λ/π^-	77.86	2.21	37.75/7
Φ/K^-	78.9	13.75	2.05/5
p/π^+	54.72	9.77	4.95/7
all strange	80.21	1.69	64.6/28

9 Conclusion

In this thesis five different particle ratio yields of central nucleus-nucleus collisions measured in particle accelerators were compared with results from a thermal model. The focus was on finding the ideal temperature at which the model gives the best description of the measured data.

For all temperatures, except for the lowest one, the best agreement was achieved with the smallest canonical volumes. Using V3 the best description of the experimental data was achieved with a double kinetic freeze-out, where the strange and non-strange particles have two different freeze-out points. For the non-strange particles we found an ideal temperature of $54.72 \pm 9.77\,\text{MeV}$ and $80.21 \pm 1.69\,\text{MeV}$ for strange particles. The sample size for both particle categories, especially non-strange, is very small. Because of this the possibility that this result is caused by the choice of the ratios can not be ruled out. Also since no ratios with net strangeness $|S| > 1$ were analyzed we can not make a statement about the existence of a triple freeze-out.

To improve the accuracy of the fits canonical volumes lower than V3 need to be explored and additional temperature in between T1 and T2 should be added. The results also imply that the canonical volume has a far bigger impact on strange particle ratios than the temperature, calculations for temperatures over $92.6\,\text{MeV}$ and under $64.8\,\text{MeV}$ might be useful to explore that connection between temperature and volume further.

Lastly it has to be mentioned that a two dimensional fit where the temperature and volume are fitted simultaneously would be the best way to find the ideal temperatures, because of the interconnectedness of those two parameters.

References

[1] Cosimo Bambi and Alexandre D. Dolgov. "The Standard Model of Particle Physics". In: *Introduction to Particle Cosmology: The Standard Model of Cosmology and its Open Problems*. Berlin, Heidelberg: Springer Berlin Heidelberg, 2016, pp. 35–52. ISBN: 978-3-662-48078-6. DOI: 10.1007/978-3-662-48078-6_3. URL: https://doi.org/10.1007/978-3-662-48078-6_3.

[2] Particle Data Group et al. "Review of particle physics". en. In: *Prog. Theor. Exp. Phys.* 2022.8 (Aug. 2022).

[3] M. Gell-Mann. *A schematic model of baryons and mesons*. 8th ed. Physical Review Letters, 1964.

[4] D. Greenberger, K. Hentschel, and F. Weinert. *Color Charge Degree of Freedom in Particle Physics*. Springer, 2009.

[5] D. J. Gross and F. Wilczek. *Ultraviolet behavior of non-abelian gauge theories*. 30th ed. Physical Review Letters, 1973.

[6] H.D. Politzer. *Reliable perturbative results for strong interactions*. 30th ed. Physical Review Letters, 1973.

[7] Maher et al. "Theoretical characterization of the Photons Emission at Annihilation Quarks Interaction". PhD thesis. Mar. 2021.

[8] Wojciech Florkowski. *Basic phenomenology for relativistic heavy-ion collisions*. World Scientific, 2010.

[9] *The Millennium Prize Problems*. URL: https://www.claymath.org/millennium-problems/.

[10] Arthur Jaffe and Edward Witten. "Quantum Yang-Mills theory". In: *The millennium prize problems* 1 (2006), p. 129.

[11] Toshihiro Nonaka. "Conserved Charge Fluctuations from RHIC BES and FXT". In: *Universe* 10 (Jan. 2024), p. 49. DOI: 10.3390/universe10010049.

[12] Rolf Hagedorn. "The long way to the statistical bootstrap model: 1994". In: *Melting Hadrons, Boiling Quarks - From Hagedorn Temperature to Ultra-Relativistic Heavy-Ion Collisions at CERN*. Cham: Springer International Publishing, 2016, pp. 139–178.

[13] J. C. Collins and M. J. Perry. "Superdense matter: Neutrons or asymptotically free quarks?" In: *Phys. Rev. Lett.* 34.21 (May 1975), pp. 1353–1356.

[14] *New State of Matter created at CERN*. URL: https://home.cern/news/press-release/cern/new-state-matter-created-cern.

[15] Hui Wang. “Study of particle ratio fluctuations and charge balance functions at RHIC”. In: (2013). eprint: 1304.2073 (nucl-ex).

[16] Tim Stellhorn. “Description of particle production in pp, p–Pb and Pb–Pb collisions at the LHC using PYTHIA”. Master’s thesis. Westfälische Wilhelms-Universität Münster, 2023. URL: https://www.uni-muenster.de/imperia/md/content/physik_kp/stellhorn2023.pdf.

[17] Raimond Snellings. “Elliptic flow: a brief review”. In: *New J. Phys.* 13.5 (May 2011), p. 055008.

[18] Dr. Vladislav Borisov. *Thermodynamik und Statistische Mechanik - Theoretische Physik V*. 2017. URL: https://itp.uni-frankfurt.de/~gros/Vorlesungen/TD/.

[19] A Andronic, P Braun-Munzinger, and J Stachel. “Hadron production in central nucleus-nucleus collisions at chemical freeze-out”. In: *arXiv [nucl-th]* (2005).

[20] Iqbal Mohi Ud Din et al. “Collision energy dependence of particle ratios and freeze-out parameters in ultra relativistic nucleus nucleus collisions”. In: *arXiv [hep-ph]* (2024).

[21] Peter Braun-Munzinger et al. “Properties of hot and dense matter from relativistic heavy ion collisions”. In: *arXiv [nucl-th]* (2015).

[22] Giorgio Torrieri et al. “SHARE: Statistical hadronization with resonances”. In: *arXiv [nucl-th]* (2004).

[23] Granddon D Yen et al. “Excluded volume hadron gas model for particle number ratios in A+A collisions”. In: *arXiv [nucl-th]* (1997).

[24] P Braun-Munzinger, I Heppe, and J Stachel. “Chemical equilibration in Pb+Pb collisions at the SPS”. In: *arXiv [nucl-th]* (1999).

[25] F Becattini and U Heinz. “Thermal hadron production in pp and $p\bar{p}$ collisions”. In: *arXiv [hep-ph]* (1997).

[26] P Braun-Munzinger, K Redlich, and J Stachel. “Particle Production in Heavy Ion Collisions”. In: *arXiv [nucl-th]* (2003).

[27] Anton Andronic. private communication.

[28] Anton Andronic et al. “Decoding the phase structure of QCD via particle production at high energy”. en. In: *Nature* 561.7723 (Sept. 2018), pp. 321–330.

[29] Timothy G Feeman. *Applied linear algebra and matrix methods*. en. Springer undergraduate texts in mathematics and technology. Cham: Springer International Publishing, 2023.

[30] Timothy G Feeman. “Least squares and matrix geometry”. en. In: *Springer Undergraduate Texts in Mathematics and Technology*. Springer undergraduate texts in mathematics and technology. Cham: Springer International Publishing, 2023, pp. 167–198.

[31] M. Waqas and G. X. Peng. “Study of Dependence of Kinetic Freezeout Temperature on the Production Cross Section of Particles in Various Centrality Intervals in Au Au and Pb Pb Collisions at High Energies”. In: (2021). DOI: 10.3390/e23040488. eprint: arXiv:2104.12067.

[32] K. Bugaev et al. “Chemical freeze-outs of strange and non-strange particles and residual chemical non-equilibrium”. In: (Dec. 2013).

[33] M Waqas et al. “Decoupling of non-strange, strange and multi-strange particles from the system in Cu–Cu, Au–Au and Pb–Pb collisions at high energies”. en. In: *Chin. J. Phys.* 77 (June 2022), pp. 1713–1722.

A Appendix

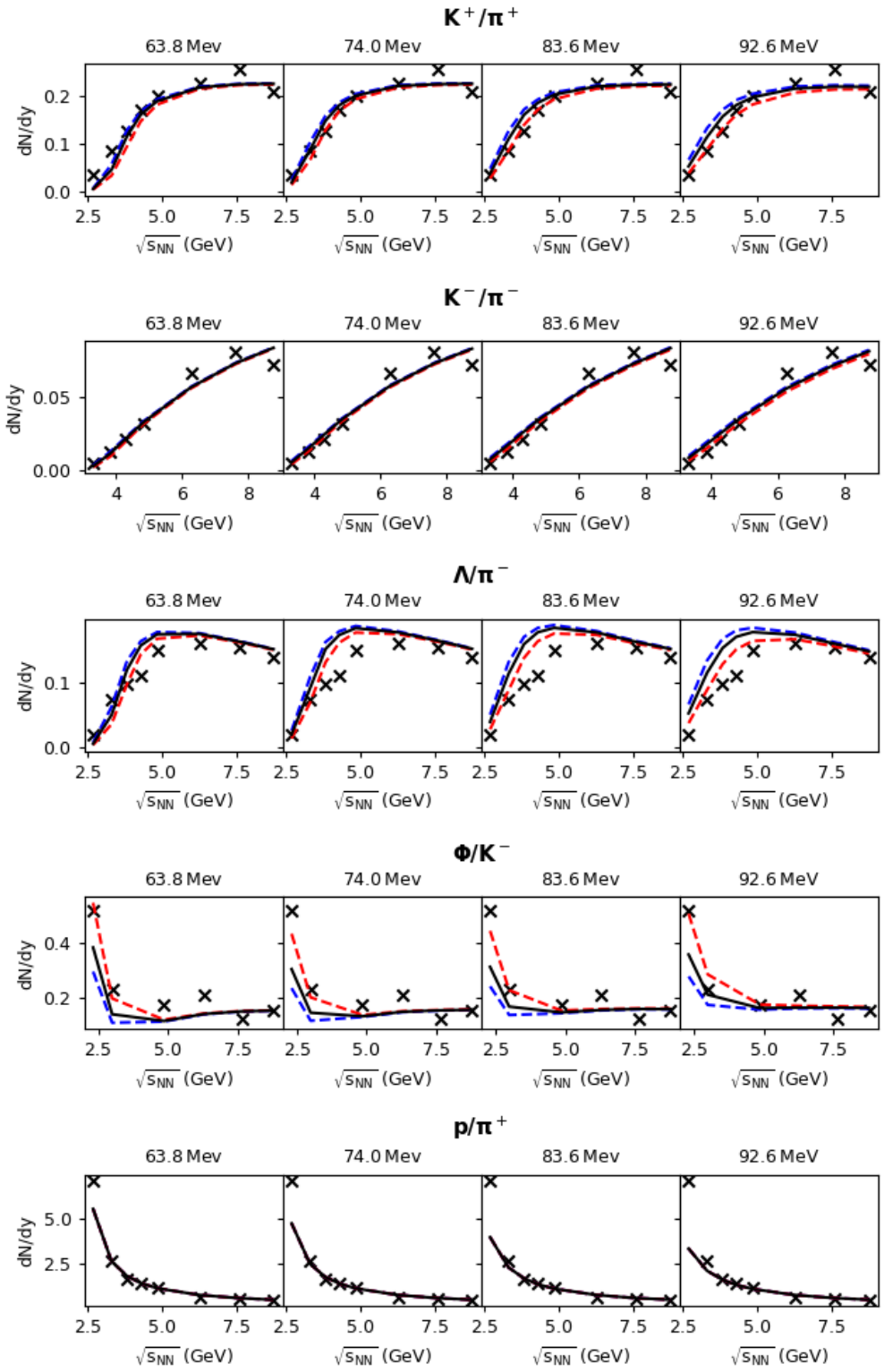

Figure 13: Comparison of experimental data (X) to Theoretical data of energies smaller than 10 GeV, where black is the mean Volume V, blue $V + \Delta V$ and red $V - \Delta V$

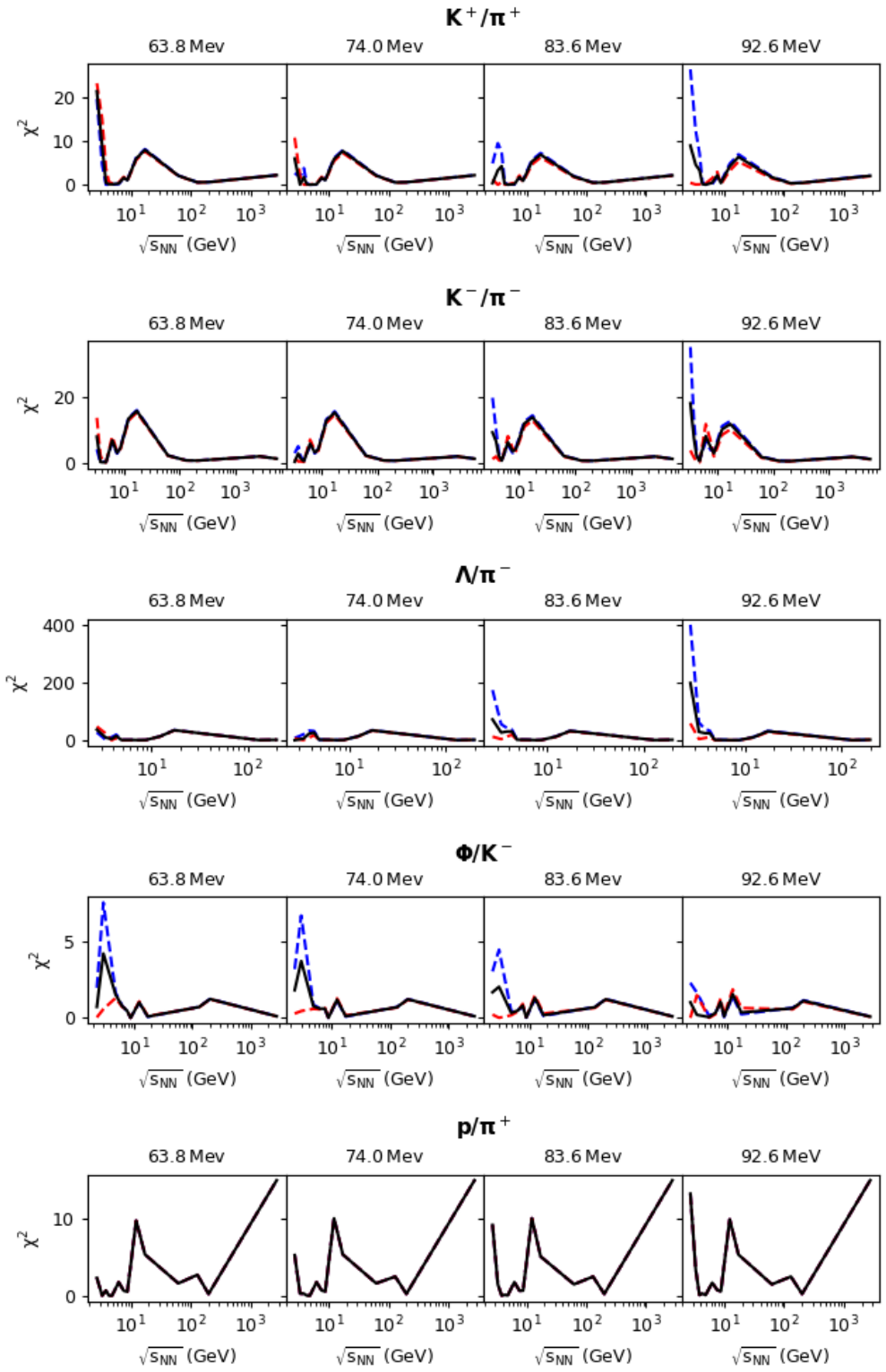

Figure 14: Error of theoretical value for all energies separate for V1 (black), V2 (blue) and V3 (red)

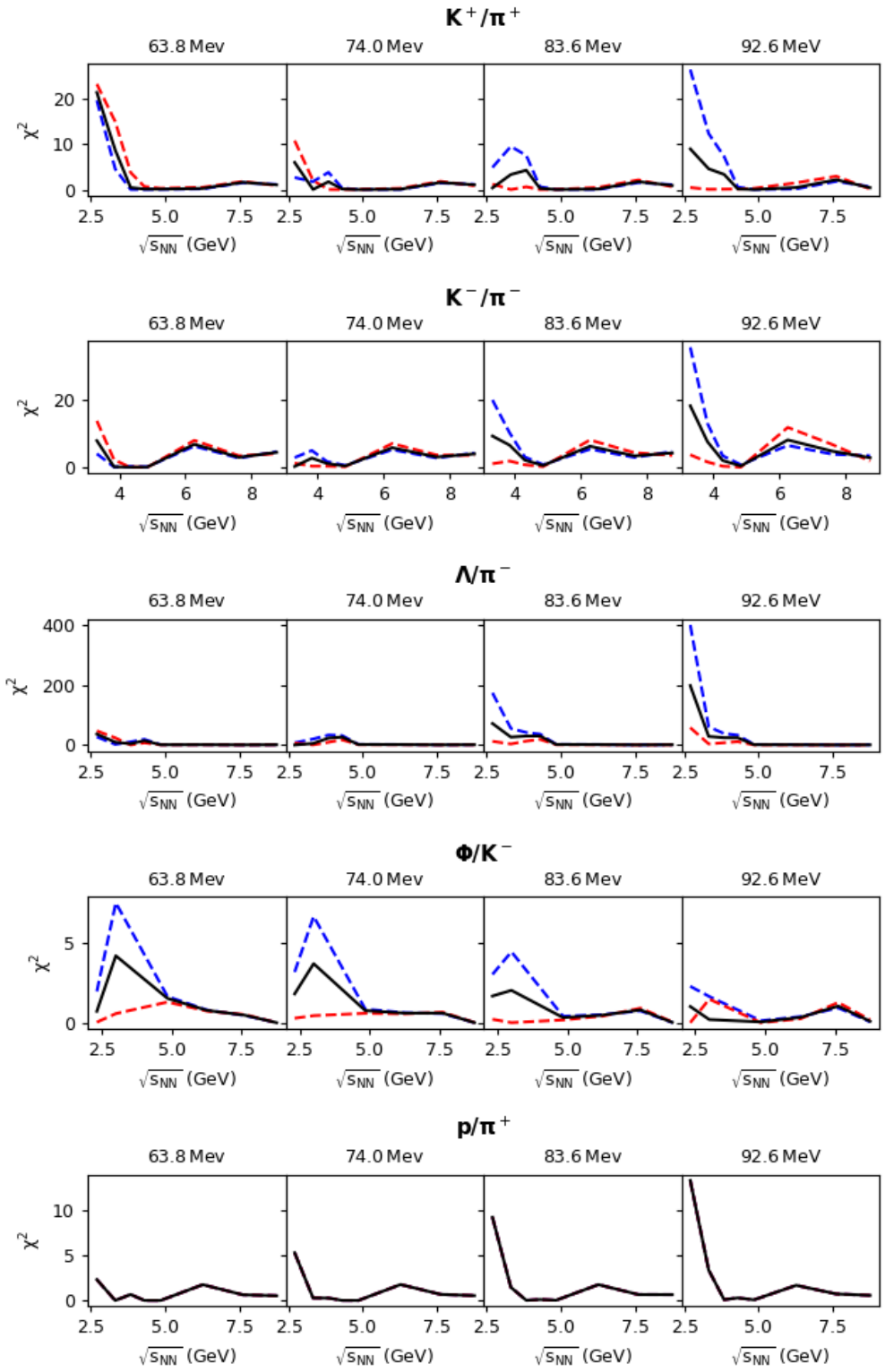

Figure 15: Error of theoretical value for all energies below 10 GeV separate for V1 (black), V2 (blue) and V3 (red)

B Declaration of Academic Integrity

I hereby confirm that this thesis, entitled "Statistical model fits of hadron ratios in nucleus-nucleus collisions", is solely my own work and that I have used no sources or aids other than the ones stated. All passages in my thesis for which other sources, including electronic media, have been used, be it direct quotes or content references, have been acknowledged as such and the sources cited.
I am aware that plagiarism is considered an act of deception which can result in sanction in accordance with the examination regulations.
I confirm that I am aware that my work may be cross-checked with other texts to identify possible similarities and that it may be stored in a database for this purpose.
I confirm that I have not submitted the following thesis in part or whole as an examination paper before.

Münster, 4.5.25
Place, Date

T. Gaintges
Signature